BIOCHEMISTRY
including biophysical chemistry & molecular biology

Article

pubs.acs.org/biochemistry

Steric Zipper Formed by Hydrophobic Peptide Fragment of Syrian Hamster Prion Protein

Hsin-Mei Cheng, Tim W. T. Tsai, William Y. C. Huang, Hsin-Kuan Lee, Huei-Ying Lian, Fang-Chieh Chou, Yun Mou, and Jerry C. C. Chan*

Department of Chemistry, National Taiwan University, No. 1, Section 4, Roosevelt Road, Taipei 106, Taiwan

Supporting Information

ABSTRACT: Steric zippers, where the residues of two neighboring β-sheet layers are tightly interdigitated, have been proposed as fundamental structural units of amyloid fibrils by Eisenberg and co-workers. The steric zipper formed by polypeptides containing the palindromic sequence AGAAAAGA has a distinctive feature that the distance between two interdigitated β-sheet layers is comparable to the interstrand distance of the individual β-sheet. This structural motif is of great interest in the study of prion disease because the AGAAAAGA sequence is highly conserved in prion proteins of different species. In this work, the amyloid fibrils formed by the polypeptides of PrP(113−127), viz. Ac-AGAAAAGAVVGGLGG-NH_2, are taken as the model compound to investigate the biophysical principles governing the steric zipper formation. The target fibrils adopt the structural motif of class 7 steric zipper, which is formed by stacking of antiparallel β-sheet layers with residue 117 + k forming backbone hydrogen bonds to residue 120 − k. Implication of our results in the infectivity of scrapie prion is briefly discussed.

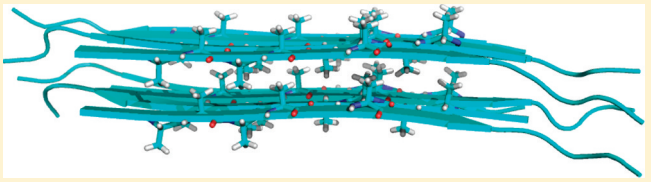

Amyloid fibrils are filamentous insoluble protein aggregates closely related to many fatal neurodegenerative diseases.[1,2] To date, solid-state NMR (SSNMR) has become the major analytical tool to unravel the structural details of amyloid fibrils.[3,4] The hydrogen bond registry of the β-sheet layer, the existence of salt bridge, the quaternary contact between β-sheet layers, and the formation of polar zipper can be determined by various cleverly designed SSNMR experiments.[5] Although the noncrystalline nature of amyloid fibrils generally precludes the use of diffraction techniques for their structural elucidation, Eisenberg and co-workers have recently determined by X-ray microcrystallography the crystal structures of GNNQQNY and a series of other amyloidogenic polypeptides,[6,7] from which the term "steric zipper" is coined to describe the dry surface between two tightly interdigitated β-sheets. In particular, a total of eight classes of steric zipper have been categorized, reflecting the various relative orientations of the two stacking β-sheet layers.[7]

In the structural model of Aβ_{1-40}, a direct contact between β-sheet layers have been proposed based on the experimental constraints on the fibril dimension,[8] which was subsequently verified by SSNMR measurements.[9] Using cryoelectron microscopy, paired β-sheet regions was observed for Aβ_{1-40} fibrils at a resolution of 8 Å.[10] Strictly speaking, it remains uncertain whether the paired β sheets in Aβ_{1-40} are tightly interdigitated by side-chain−side-chain interactions. Apparently, the first illustration of the notion of interdigitated β-sheets can be traced to the molecular dynamics (MD) simulations of the octamers formed by AGAAAAGA.[11] This study shows that the most stable octamer is formed by the parallel stacking of two antiparallel β sheets, and the stability of the octamer is mainly due to the hydrophobic interactions among the alanine residues. The formation of steric zipper is also suggested in the structural model constructed for MoPrP$_{106-126}$ fibrils, which contains two four-stranded parallel β-sheets tightly packed together by hydrophobic interactions.[12] A similar observation has been reported for the MD simulations of ccβ-Met amyloid fibrils, where the layer−layer structural constraints were inferred from X-ray diffraction data.[13] The first direct detection of the layer−layer distance of steric zipper in amyloid fibrils was given in the SSNMR study of PrP$_{109-122}$ fibrils,[14] where the interlayer distance was found to be ∼5 Å. Later, steric zipper formation was also found in hAIPP$_{20-29}$ fibrils[15,16] and PrP$_{106-126}$ fibrils[17] by SSNMR spectroscopy.

On the basis of the structural polymorphs observed for the microcrystals formed by fragments of prion and other amyloid proteins, packing and segmental polymorphisms of steric zippers have been postulated as the structural origin of prion strains.[18] Although structural polymorphism is commonly observed in amyloid fibrils,[19,20] it is very challenging to verify the above proposition by elucidating the molecular structures of individual polymorphs. To shed more light on this intriguing hypothesis, one may compare the molecular structures of the steric zippers formed by different peptide sequences so that the underlying biophysical principles governing the zipper formation process may be unraveled. The sequence of AGAAAAGA (residues 113−120) is highly conserved in prion proteins of different species. This palindrome sequence

Received: May 9, 2011
Revised: June 30, 2011
Published: July 13, 2011

is in the vicinity of the β1 region (residues 127−132) of cellular prion protein (PrP^C), which has been suggested as the nucleation site for the conformational transition of PrP^C to its pathogenic state, i.e., the scrapie prion (PrP^{Sc}).[21,22] Consequently, it is interesting to investigate whether or not peptide fragments encompassing the sequence of AGAAAAGA would form different classes of steric zipper. Accordingly, the $PrP_{106-126}$ fibrils comprise in-registered parallel β-sheet layers adopting the structural motif of class 1 steric zipper.[17] For the $PrP_{109-122}$ fibrils, it has been unequivocally shown that the fibrils contain antiparallel β-sheets with the A117 residues aligned to form a linear chain in the direction of the fibril axis. However, it is not trivial to discern the packing mode of two antiparallel β-sheet layers and the reported experimental data can only corroborate the formation of steric zipper in $PrP_{109-122}$ fibrils.[14] In this work, we have characterized the structural features of the fibrils formed by the 113−127 fragment of prion protein ($PrP_{113-127}$), viz. Ac-AGAAAAGAVVGGLGG-NH_2. By a careful analysis of the solid-state NMR data and the subsequent all-atom MD simulations, we find that $PrP_{113-127}$ fibrils adopt the class 7 steric zipper. That is, the two stacking antiparallel β sheets have the same orientation along the fibril axis. Together with the findings that class 1 steric zipper is formed in $PrP_{106-126}$ fibrils,[17] we can safely conclude that the palindromic sequence AGAAAAGA has a strong propensity to form steric zipper, but the β-sheet organization and the packing mode of the neighboring β-sheet layers are very sensitive to the local environment of the palindrome sequence. In view of other biochemical results that the AGAAAAGA region is likely to be solvent exposed in PrP^{Sc},[23,24] the hydrophobic interaction of AGAAAAGA may be associated with the infectivity of PrP^{Sc}.

MATERIALS AND METHODS

Sample Preparation. All the chemicals were obtained from NovaBiochem (Merck KGaA, Darmstadt, Germany) unless stated otherwise. $PrP_{113-127}$ peptides, with the sequence Ac-AGAAAAGAVVGGLGG-NH_2, were synthesized on an automated Odyssey microwave peptide synthesizer (CEM Corp., Matthews, NC), using a Rink amide resin (0.6 mequiv/g substitution level), and 9-fluorenylmethoxycarbonyl (FMOC) chemistry with 2-(1*H*-benzotriazole-1-yl)-1,1,3,3-tetramethyluronium hexafluorophosphate activation. The synthesis scale was 0.1 mmol, with a 2-fold and 5-fold excess for isotopically labeled and unlabeled amino acid, respectively. For all residues, the coupling step was carried out for 2 h at room temperature. Crude peptides were cleaved from the synthesis resin using standard protocols (reaction for 105 min in 95% trifluoroacetic acid (TFA) with 2.5% deionized (DI) water and 2.5% triisopropylsilane), which were then precipitated in cold *tert*-butyl methyl ether (TBME). Precipitated peptides were washed three times with cold TBME and then lyophilized. The crude material was purified by high-performance liquid chromatography at 50 °C, using a water/acetonitrile gradient with 0.1% TFA and a preparative scale Vydac C18 reverse-phase column. Samples of 5 mg per injection were dissolved in 100 μL of TFA and then diluted to 5 mL with 10% acetonitrile in DI water before being injected into the column. Fractions containing the target product were frozen in liquid nitrogen immediately after being collected. Peptide purity was at least 90% as determined by MALDI-TOF mass spectrometry. The yield of purified peptide was ∼25%. ^{13}C- and ^{15}N-labeled amino acids with FMOC protection were obtained from Cambridge Isotope Laboratories (Andover, MA), CortecNet (Tilleuls, France), and Isotec (St. Louis, MO). Fibril samples were formed by dissolution of purified peptides in 20 mM Hepes buffer with addition of 0.01% NaN_3. The peptide concentration was set to 880 μM. After sonication in ice bath for 1 min (5 W), the sample was incubated at 37 °C for various periods. The sample for subsequent measurements was incubated for 3 days.

Transmission Electron Microscopy (TEM). An aliquot (10 μL) of fibril sample was suspended on a carbon-coated copper grid for 1 min. Aliquots (10 μL) of DI water were added and blotted for three times to remove the salt. After staining with 2% phosphotungstic acid for 1 min, TEM images were recorded using a Hitachi H-7100 electron microscope operated at 80 kV.

Fourier Transform Infrared (FT-IR). Transmittance FT-IR spectra were collected using a Perkin-Elmer (System 2000) spectrometer in the range of 1000−4000 cm^{-1}. The samples were recorded in KBr pellets at room temperature. The frequency scale was calibrated with the measurement of succinic acid.

Solid-State NMR. For NMR measurements, the salts of the fibril samples were first removed by dialysis for 20 h (Cellu Sep H1 part #0550-40 MWCO:5000) and then lyophilized. All NMR experiments were carried out at ^{13}C and ^{1}H frequencies of 75.5 and 300.1 MHz, respectively, on a Bruker DSX300 NMR spectrometer equipped with a commercial 2.5 mm double-resonance probe. The magic-angle spinning (MAS) frequency variation was limited to ±3 Hz using a commercial pneumatic control unit (Bruker, MAS II). Each fibrillized sample of ∼5 mg was packed in the middle one-half of the rotor volume using Teflon spacers for subsequent measurements. Typically, during the cross-polarization contact time (1.5 ms), the ^{1}H nutation frequency was set to 50 kHz and that of ^{13}C was ramped through the Hartmann−Hahn matching condition. Unless stated otherwise, continuous-wave and XiX[25] proton decouplings of 100 kHz were applied during recoupling periods and the t_2 acquisition, respectively. To reduce the sample heating due to fast MAS spinning, a stream of dry cooling air at −11 °C (800 L/h) was used to keep the sample temperature at around 30 °C, calibrated by measurements on lead(II) nitrate. ^{13}C NMR chemical shifts were referenced to tetramethylsilane, using adamantane as the secondary reference standard.

$^{13}C/^{13}C$ chemical shift correlation spectra were measured at an MAS frequency of 25.0 kHz using the fpRFDR technique[26] with a mixing time of 3.2 ms. During the fpRFDR recoupling period, the ^{13}C π pulses were set to 12 μs. The ^{13}C $\pi/2$ pulses flanking the fpRFDR pulse blocks were set to 4 μs. Chemical shift and line width data were obtained by fitting each cross-peak to a Gaussian using the package NMRPipe[27] and Sparky.[28] $^{13}C-^{13}C$ dipolar recoupling measurements were carried out with the constant-time fpRFDR (fpRFDR-CT) technique,[29] at an MAS frequency of 20.0 kHz. The effective dipolar dephasing period was from 0 to 33.6 ms in steps of 2.4 ms. Continuous-wave proton decoupling was 130 kHz during the recoupling period. The C′ and C^β fpRFDR-CT data were obtained separately by placing the rf transmitter frequency near the C′ and C^β signals, respectively. The number of transients accumulated for each fid was 512. Total acquisition time for each fpRFDR-CT data set was ∼8 h, using a 4 s recycle delay. Numerical analyses of the fpRFDR-CT data were carried out

using SIMPSON (version 1.1.0)[30] and SPINEVOLUTION (version 3.4).[31]

Molecular Modeling. MD simulations were carried out using the program TINKER (version 4.2).[32] An antiparallel β sheet was prepared by arranging four β strands of $PrP_{113-127}$ according to the configuration determined by isotope-edited FT-IR measurements. The interstrand distance was set to 4.8 Å, and the backbone torsion angles of all the residues were restrained to ϕ and ψ values of $-140°$ and 140°, respectively. Another similarly prepared β sheet was then stacked in a parallel fashion, resulting in a layer distance of 7 Å. All atoms of the system were considered explicitly under a periodic boundary condition of 150 × 150 × 20 Å, and their interactions were calculated by using the Amber99 force field.[33] The solvent-accessible-surface-area approach was chosen as our solvent model.[34] A distance cutoff of 9 Å was set for all nonbonded interactions. Long-range electrostatic interactions were evaluated by the smooth particle-mesh Ewald method.[35] The RATTLE algorithm was used to constrain all chemical bonds containing H atoms to their ideal bond lengths.[36] The time step in the MD simulations was 1−2 fs. Figures 7 and 8 were prepared using PyMol[37] and MolMol,[38] respectively.

RESULTS

Observation of Amyloid Fibrils Formed by PrP(113−127). The TEM image of the $PrP_{113-127}$ fibrils is shown in Figure 1. The sample typically contains short filaments forming

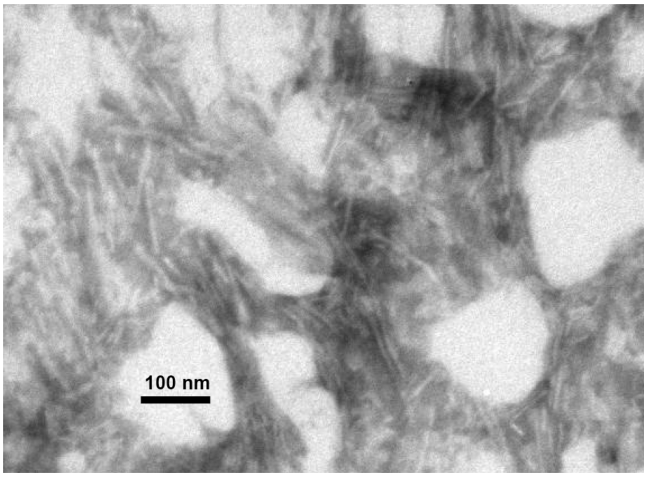

Figure 1. TEM image of the $PrP_{113-127}$ fibrils after incubation for 3 days.

a random meshwork (length ≤150 nm). We have shown previously that the amyloid fibrils formed by the $PrP_{109-122}$ fragment can be obtained within 1 day, and the morphology of the fibrils is very similar to what we have shown in Figure 1.[14] Because the peptide sequence of $PrP_{113-127}$ contains hydrophobic residues only, we expect that the structure of $PrP_{113-127}$ fibrils also adopts the motif of steric zipper, as in the case of $PrP_{109-122}$.

β-Sheet Organization of the PrP(113−127) Fibrils. Generally speaking, the splitting of the amide I band (consisting primarily of CO stretching) into stronger and weaker bands at ca. 1630 and 1695 cm^{-1}, respectively, is a good indication for antiparallel β-sheet structures. Infrared spectroscopy has been extensively used to study amyloid fibrils.[39] Interestingly, a very minor absorption at ca. 1696 cm^{-1} has also been observed for the fibrils of $A\beta_{1-40}$,[40] which has a parallel β-sheet structure.[41] Thanks to the high-resolution structure obtained by solid-state NMR spectroscopy, this puzzling observation has been rationalized by the turn structure of $A\beta_{1-40}$ fibrils.[8] Although such a turn structure is unlikely to occur in a short polypeptide, the so-called class 1 steric zipper could well be formed by the stacking of two parallel β-sheet layers in an antiparallel fashion. This structural motif has indeed been observed for the $PrP_{106-126}$ fibrils.[17] Therefore, the splitting of the amide I band may not be an unequivocal spectral marker for an antiparallel β-sheet structure in our case. On the other hand, isotope-edited FT-IR spectroscopy is a powerful technique to probe the hydrogen-bond registry in amyloid fibrils formed by short peptide fragments.[42−44] In brief, if the site-specific ^{13}C-labeled carbonyl carbons are aligned along the fibril axis, the isotope-shifted ^{13}C amide I′ band will have a further red shift by ∼8−10 cm^{-1} due to the coupling of the transition-dipole moments of the amide I′ modes.[42] On the contrary, simulations show that parallel alignment of ^{13}C-labeled carbonyl carbons of two stacking β-sheet layers would induce a blue shift of the amide I′ band.[45] Figure 2 shows the FT-IR spectra measured for our fibril samples with different ^{13}C isotopic labeling. The labeling scheme is given in Table 1. For the samples of *AA*1 and *AG*1, where the carbonyl carbons of A118 and G119 are ^{13}C-enriched, respectively, the amide I′ band occurs at 1696, 1634, and 1610 cm^{-1}. The corresponding low-frequency components observed for the aligned and unaligned residues in the $PrP_{109-122}$ fibrils are found at 1604 and 1612 cm^{-1}, respectively.[14] Therefore, we conclude that neither the A118 nor the G119 is aligned along the fibril axis. Consequently, the hydrogen bond registry of the $PrP_{113-127}$ fibrils is hypothesized as illustrated in Figure 3, which represents a reasonable compromise between the number of hydrogen bonds and the extent of the steric zipper along the strand direction. To test our hypothesis, we have prepared the fibril sample *AA*2 with ^{13}C labeling at the carbonyl carbons of A117 and A120. If our hypothesis is correct, the coupling of the transition-dipole moment of the two aligned ^{13}CO stretching modes will produce a further red shift of the corresponding absorption peak.[42] As shown in Figure 2, the ^{13}C amide I′ band of *AA*2 is indeed shifted to 1604 cm^{-1}. This red shift by 6 cm^{-1} lends strong support to our proposed β-sheet structure shown in Figure 3. That is, residue 117 + k forms backbone hydrogen bonds to residue 120 − k in $PrP_{113-127}$ fibrils, where k is an integer.

Evidence for the Formation of Steric Zipper. NMR chemical shifts and line width data obtained from the two-dimensional $^{13}C/^{13}C$ chemical shift correlation spectra are summarized in Table 2. Only the ^{13}C chemical shifts of selected residues were measured. On the basis of the line width data, we can conclude that the structural order of the residues from A113 to A120 is relatively high, whereas a significant structural disorder is observed near the C-terminus. The secondary shifts calculated for the residues in the region of the palindromic sequence are consistent with β-sheet conformation. As an independent verification of the hypothesis shown in Figure 3, we have measured the $^{13}C-^{13}C$ correlation spectrum of the sample of *AA*3, where the C′ of A117 and C^{β} of A120 are ^{13}C labeled (see the Supporting Information). A pair of strong correlation peaks are indeed observed, proving that these two ^{13}C species are in close proximity. Figure 4 shows the $^{13}C-^{13}C$

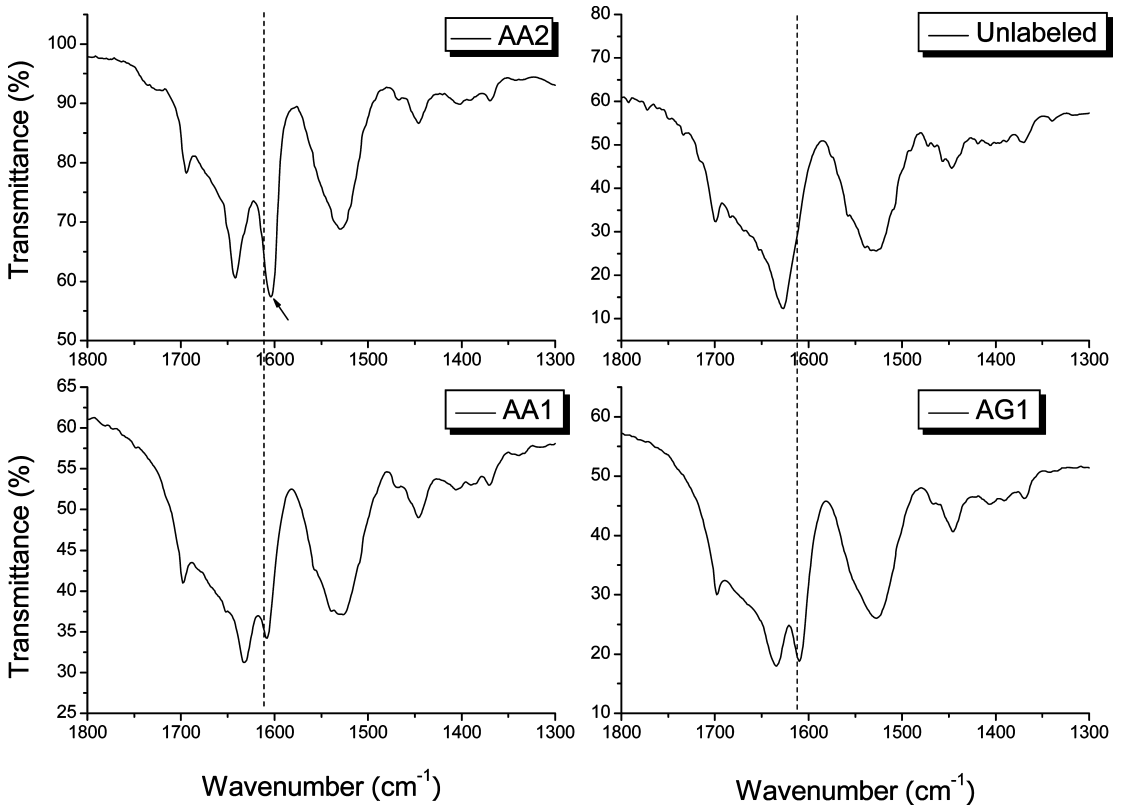

Figure 2. FT-IR spectra measured for $PrP_{113–127}$ fibrils. The C′ atoms are ^{13}C-labeled at A118 (*AA*1), G119 (*AG*1), and simultaneously at A117 and A120 (*AA*2). The dashed line denotes the position at 1612 cm^{-1}, which corresponds to the scenario of unaligned residues. The arrow indicates the significant red shift observed for the *AA*2 sample.

Table 1. Isotopic Labeling of $PrP_{113–127}$ Fibril Samples

sample	labeling scheme	measurements
AV	uniform ^{15}N and ^{13}C labeling of A113,V122	SSNMR
AVL	uniform ^{15}N and ^{13}C labeling of A115, V121, L125	SSNMR
*AA*1	^{13}C labeling of C^{β} at A113 and ^{13}C labeling of C′ at A118	FT-IR/ SSNMR
*AA*2	^{13}C labeling of C′ at A117 and A120	FT-IR
*AA*3	^{13}C labeling of C^{β} at A120 and ^{13}C labeling of C′ at A117	FT-IR/ SSNMR
*AG*1	^{13}C labeling of C^{β} at A117 and ^{13}C labeling of C′ at G119	FT-IR/ SSNMR
*AG*2	^{13}C labeling of C^{β} at A116 and ^{13}C labeling of C′ at G123	FT-IR/ SSNMR
AL	^{13}C labeling of C^{β} at A118 and ^{13}C labeling of C′ at L125	FT-IR/ SSNMR
A	^{13}C labeling of C^{β} at A120	SSNMR

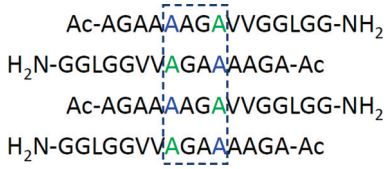

Figure 3. Hypothetical antiparallel *β*-sheet organization of the $PrP_{113–127}$ fibrils. The residues highlighted in blue and green correspond to A117 and A120, respectively.

correlation spectrum measured for the *AVL* sample. For A115 there is only one set of C^{α} and C′ chemical shifts, but the C^{β} signal has two sharp components of chemical shifts equal to

Table 2. ^{13}C NMR Chemical Shift and Line Width Data (ppm) for ^{13}C-Labeled Sites in $PrP_{113–127}$ Fibrils[a]

	fibrils (samples incubated for 3 days)			
residue	C′ δ, $\Delta\nu_{1/2}$	C^{α} δ, $\Delta\nu_{1/2}$	C^{β} δ, $\Delta\nu_{1/2}$	sample
A113	172.9, 2.3	48.7, 2.6	20, 4	*AV*
A115	171.6, 2.1	48.7, 1.5	20.4, 2.0 (57%)	*AVL*
			22.3, 1.7 (43%)	
A116			20.6, 1.6 (59%)	*AG*2
			22.5, 1.5 (41%)	
A117	172.6, 2.0		22.8, 1.6 (60%)	*AG*1, *AA*3
			24.8, 1.4 (40%)	
A118	173.2, 2.0		21.0, 1.8 (64%)	*AL*, *AA*1
			23.8, 1.7 (36%)	
G119	170.1, 2.2			*AG*1
A120			20.5, 2.0 (62%)	*AA*3
			22.9, 2.0 (38%)	
V121	170, 5	56.9, 2.2	34, 3.4	*AVL*
V122	173, 3	57, 5	33, 4	*AV*
G123	171, 4			*AG*2
L125	174, 5	51, 7	–, –	*AVL*

[a]The volume ratios of the doublets were determined by Sparky. No line broadening was applied before the Fourier transformation.

20.4 and 22.3 ppm—both of which are more deshielded than the random coil value.[46] Additional measurements show that the signal splitting of C^{β} is found for all alanines in the palindromic region except for A113, which is at the N-terminus. Such C^{β} signal splitting, reflecting two different quaternary contacts of the methyl groups, can be attributed to the difference in the magnetic susceptibility of the hydrophobic

dx.doi.org/10.1021/bi200712z|*Biochemistry* 2011, 50, 6815–6823

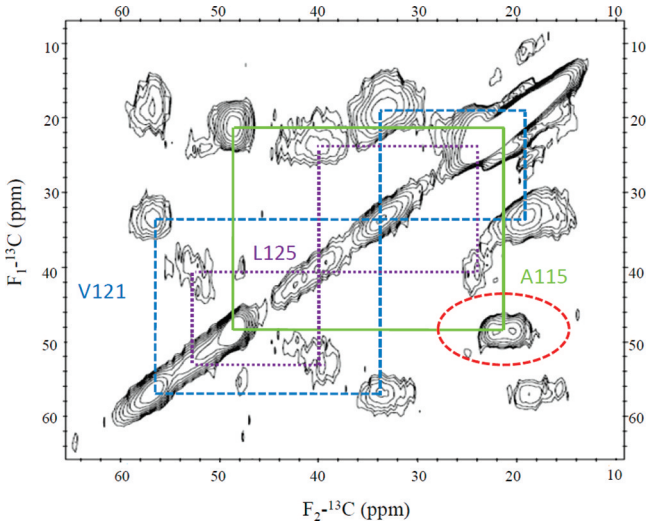

Figure 4. $^{13}C-^{13}C$ correlation spectrum of the *AVL* sample, where the residues at A115, V121, and L125 of $PrP_{113-127}$ fibrils are ^{13}C uniformly labeled. The technique of fpRFDR was used, and the mixing time was set to ca. 3 ms. The region highlighted by an elliptical dashed line denotes the spectral marker of steric zipper of class 2, 4, 6, 7, or 8. Other classes of steric zipper would give one set of signal only.

core and the hydrophilic surface. The two peak components of each doublet have a volume ratio of about 60:40, which is somewhat different from the ideal value of 50:50. This phenomenon is presumably due to the stacking of more than two β-sheet layers. As an independent verification of our interpretation, Figure 5 shows the $^{13}C-^{13}C$ correlation

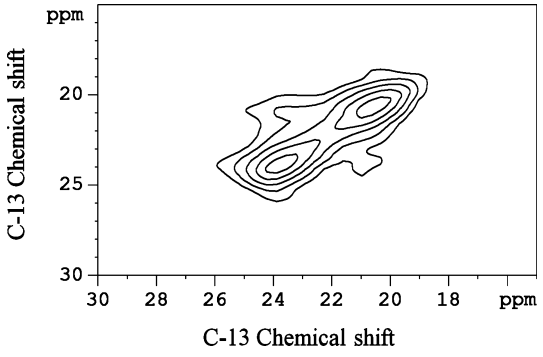

Figure 5. $^{13}C-^{13}C$ correlation spectrum of the *AL* sample, where the C^{β} at A118 is ^{13}C-labeled. Only the region of the C^{β} signals is shown. The mixing time was set to 300 ms, using the PDSD technique.[54] The spinning frequency was set to 15 kHz.

spectrum of the *AL* sample, where the cross-correlation peaks between the two C^{β} signals of A118 are clearly observed. Therefore, the C^{β} signal splitting cannot be explained by the presence of more than one fibril structure.

To determine the distance between the two β-sheet layers, we employed the ^{13}C fpRFDR-CT technique,[29] which has been successfully applied to the studies of amyloid fibrils.[47] The measurement was carried out for the sample *A*, where the C^{β} of A120 was ^{13}C-labeled. Figure 6 shows the attenuation of the $^{13}C^{\beta}$ signal as a function of the dephasing time, which is a direct consequence of the magnetic dipole−dipole interaction between the C^{β} spins in close vicinity ($\lesssim$7 Å). The fpRFDR-

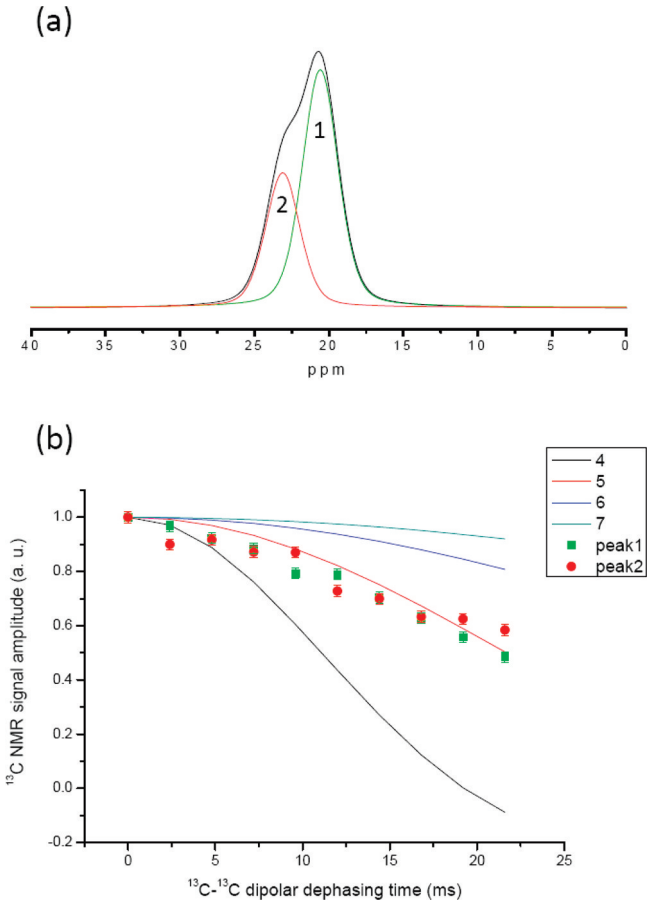

Figure 6. ^{13}C fpRFDR-CT data of the *A* sample. (a) There are two sets of C^{β} signals at A120 of $PrP_{113-127}$ fibrils. (b) Both signals have similar ^{13}C dipolar dephasing in fpRFDR-CT measurements. The lines are simulation data corresponding to a two-spin system with different internuclear distance in Å. The two peak components are arbitrarily labeled as peaks 1 and 2.

CT data were analyzed based on a two-spin system with internuclear distance (d) varied from 4 to 7 Å. The contribution from the natural abundance signals was corrected for using the procedure described in the literature.[47] By spectral deconvolution, the dephasings of the individual components of the doublets were found to be identical. From the corresponding mean-square-deviation plot, d is determined to be 5.0 ± 0.1 Å at 90% confidence level, which is consistent with the distance between the two β-sheet layers of an "alanine zipper".[14]

Deduction of the Class of Steric Zipper. On the basis of the FT-IR data, we find that our fibril samples contain antiparallel β-sheets, and therefore the steric zipper must belong to the classes of either 5, 6, 7, or 8. Figure 7 shows the models constructed for the sample *A* based on the structural motifs of class 5 and class 8 steric zippers, where the C^{β} atoms of A120 are highlighted by yellow spheres. As shown in Figure 7a, all the C^{β} atoms of A120 are located inside the steric zipper. Therefore, the class 5 steric zipper is not consistent with the observation that there are two peak components for the A120-C^{β} signals. Referring to the class 8 model (Figure 7b), the C^{β} signals of the exterior A120 residues would have little dephasing in the ^{13}C fpRFDR-CT experiments because the corresponding internuclear distances among the C^{β} atoms are longer than 7 Å.

dx.doi.org/10.1021/bi200712z | *Biochemistry* 2011, 50, 6815–6823

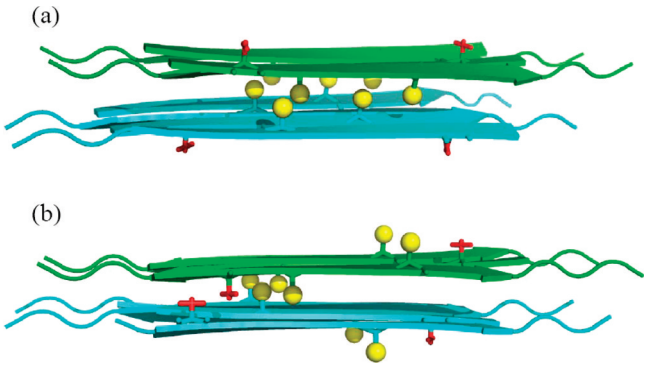

Figure 7. Schematic structures constructed based on the class 5 and class 8 steric zipper. The methyl groups of A115 of two selected peptide strands of each β-sheet layer are represented by red sticks to help illustrate the relative orientation among the peptide strands. The C^{β} atoms of A120, which are isotopically labeled in the sample *A*, are highlighted as yellow spheres. The antiparallel organization of each β-sheet is constrained by the isotope-edited FT-IR data. (a) For the class 5 model, all the yellow spheres are located in the interior region of the steric zipper, which is inconsistent with the observation that there are two $^{13}C^{\beta}$ spectral components observed for the sample *A*. (b) For the class 8 model, the shortest distance among the yellow spheres in the exterior region is longer than 7 Å. Thus, the class 8 model cannot explain the observation shown in Figure 6, where both the two C^{β} signals have the same dipolar dephasing corresponding to an internuclear distance of ~5 Å.

Therefore, the data shown in Figure 6, where both components of the A120-C^{β} signals have strong dephasing, can rule out qualitatively the validity of the class 5 and 8 models. To investigate the fidelity of the class 6 and 7 models, we have carried out MD simulations on an octamer of the $PrP_{113-127}$ peptides using implicit solvent model. This procedure is partially justified by the fact that unrestrained MD simulations can reproduce with high degree of accuracy the interlayer distance and the backbone torsion angles at the zipper region for $PrP_{109-122}$ fibrils.[14] The initial configuration of the octamer was prepared based on the class 6 or 7 steric zipper, where the hydrogen-bond registry was set in accordance to what depicted in Figure 3. Each β-sheet layer of the steric zipper was formed by four peptide strands as described in the Materials and Methods section. Energy minimization was done to relax local strains. For the class 6 steric zipper, an unrestrained NPT (constant number of particles, 1 atm, 300 K) simulation of 2 ns shows that the steric repulsion between the valine residues will destabilize the structure seriously (see the Supporting Information), and the resultant structure is not consistent with the ^{13}C fpRFDR-CT data. Therefore, the class 6 steric zipper is discarded in our case. On the other hand, the zipper region of the class 7 model remains stable after the same unrestrained NPT simulation. Consequently, the molecular model of the $PrP_{113-127}$ fibrils is constructed as follow. Initially, an NPT simulation at 300 K was performed for 2.2 ns based on the class 7 steric zipper with idealized cross-β structure, followed by another NPT simulation at 800 K for 200 ps. The interlayer distance was restrained to 5 Å with a force constant of 100 kcal/Å^2 in these two NPT simulations. After that, structures extracted at every 20 ps of the NPT trajectory at 800 K were energy minimized without any structural restraints. All the 10 structures after the final round of energy minimization are shown in Figure 8, and they have more or less the same total energy. The stability of the average structure was confirmed by an unrestrained MD simulation at 800 K for 200 ps.

DISCUSSION

In general, the hydrogen bond registries in amyloid fibrils are the consequence of a delicate balance of hydrophobic, pH-dependent electrostatic, and van der Waals interactions.[3] For our $PrP_{113-127}$ fibrils, both the C- and N-termini are capped and all the residues are hydrophobic. Therefore, one would expect that the side-chain−side-chain interaction is a strong determinant of the fibril structure. At the first glance it is quite surprising that $PrP_{113-127}$ fibrils do not adopt an in-registered parallel β-sheet structure. In addition, the number of hydrogen bonds is not maximized for the β-sheet structure as shown in Figure 3. Nevertheless, it has been shown by Ma and Nussinov that the interaction among the methyl groups buried in a hydrophobic core is the major stabilizing force for a zipper-like cluster.[11] In addition, simulations of polyalanine peptides show that the alanine side chains of an adjacent β-sheet would fit into the "pockets" on the neighboring sheet upon fibril formation.[48,49] These observations derived from in silico

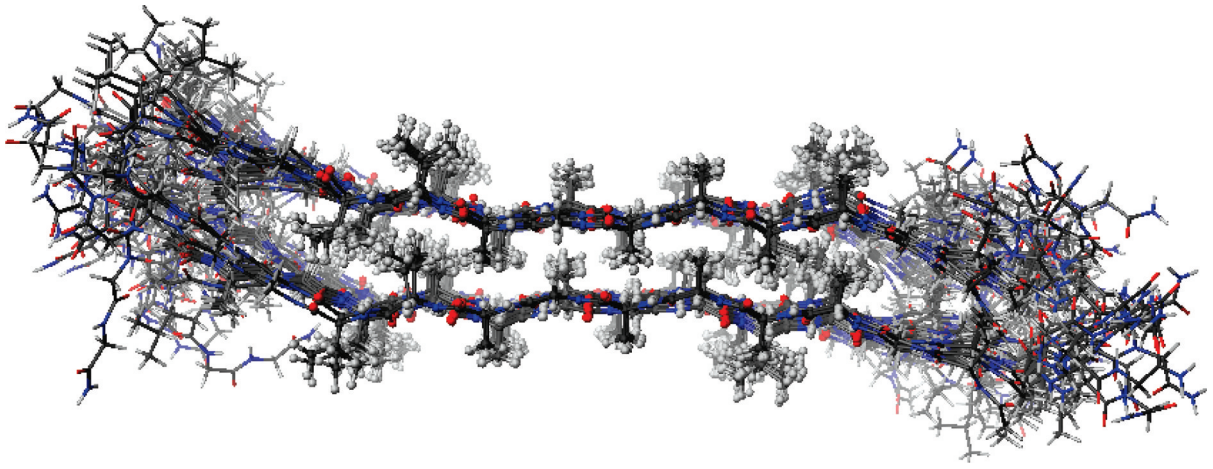

Figure 8. Structural model of the $PrP_{113-127}$ fibrils. The structure belongs to the class 7 steric zipper. The 10 overlaid structures were obtained from restrained MD simulations followed by unrestrained energy minimization.

studies are consistent with our experimental results. In other words, the stability of the $PrP_{113-127}$ fibrils is largely due to the formation of steric zipper, where the interdigitation of two β-sheet layers is formed via the tight packing of the methyl groups. Our structural model reflects a delicate balance of the following three factors including: (i) the extent of the zipper region, (ii) the number of hydrogen bonds between $PrP_{113-127}$ molecules, and (iii) the steric effect of the side chains of residues such as valine. Although steric zipper can be formed by residues with large side chains,[6,7] the zipper formed by the sequence of AGAAAAGA represents a particular tight packing of two β-sheet layers. For this "alanine zipper", other residues of larger side chains such as valine would significantly destabilize the zipper region. Our model, in which the region VVGGLGG is relatively disordered, is in line with the finding that the sequence of AGAAAAGA is highly amyloidogenic but not the VVGGLGG sequence.[50]

As discussed by Eisenberg and co-workers,[18] packing polymorphism of steric zippers has been observed for the microcrystals formed under different solution conditions. However, it is not obvious whether a unique packing mode between the neighboring β-sheet layers could be found in steric zippers of amyloid fibrils. If different modes of packing are present in the same fibril sample, the generality of the hypothesis that prion strains could be encoded by alternative packing arrangements of β-sheets may be undermined. To date, only the $PrP_{106-126}$ fibrils have been shown to adopt a unique packing mode, i.e., the class 1 steric zipper. The driving force of this antiparallel packing of two parallel β-sheets, however, is presumably due to the formation of a salt bridge between the C-terminus and the side chain of K110.[17] This somewhat nonnative salt bridge formation may not play any significant role in PrP^{Sc}. Our $PrP_{113-127}$ fibrils, on the other hand, do not contain any charged or polar residues. That is, the hydrophobic interaction among the side chains will determine which class of steric zipper is energetically the most favorable one. In retrospect, it is very interesting to find that our $PrP_{113-127}$ fibril sample can be described uniquely by the class 7 steric zipper. This observation indicates that the energy landscape of the conformational space of $PrP_{113-127}$ has significant barriers among the various packing modes. Thus, it is a plausible hypothesis that packing polymorphism of steric zipper may provide the molecular mechanism for the existence of prion strains. To probe the energy landscape of the zipper formation process, our fibril system represents an excellent model for further computational studies.

The AGAAAAGA sequence is highly conserved in prion proteins of different species.[50] Therefore, its structural role in the fibrils formed by peptides containing this palindromic sequence is of considerable interest. To date, alanine zippers centering at the region of AGAAAAGA have been observed in three different amyloidogenic fragments of prion proteins including $PrP_{106-126}$,[12,17] $PrP_{109-122}$,[14] and $PrP_{113-127}$. The strong propensity to hydrophobic interaction of AGAAAAGA is also illustrated in the PrP_{23-144} fibrils, where the region of the palindromic sequence forms the most rigid core of the fibrils.[51,52] On the other hand, a recent solid-state NMR study showed that the AGAAAAGA region is not included in the core of PrP_{23-231} fibrils.[53] Other biochemical results also show that the AGAAAAGA region is likely to be solvent exposed in PrP^{Sc}.[23,24] Apparently, the overall structural stability of PrP^{Sc} can provide the necessary free energy required to expose the AGAAAAGA region to the solvent. These somewhat surprising findings lead to a speculation that the hydrophobic interaction of the AGAAAAGA region is strong enough for PrP^{Sc} to "capture" monomeric cellular prion protein, which would be subsequently converted to PrP^{Sc}. This hypothesis is consistent with the fact that the N-terminal fragment 23−120 of PrP^{C} is flexibly disordered.[22] Although it is far from clear what the exact mechanism of the transmission pathway of prion disease is, the hypothesis discussed here may deserve further investigations.

CONCLUSION

Structural elucidation of steric zippers formed by interdigitation of alanine residues are challenging because the interlayer distance is quite similar to the distance between two neighboring strands within the same β-sheet layer. We have successfully exploited isotope-edited FT-IR and homonuclear ^{13}C dipolar dephasing, in conjunction with MD simulations, to build a structural model for $PrP_{113-127}$ fibrils. The results show that $PrP_{113-127}$ fibrils adopt the structural motif of the class 7 steric zipper. The interlayer distance at the zipper region is ~5 Å. The stability of the $PrP_{113-127}$ fibrils is largely due to the formation of the zipper region. Our model suggests that fibril formation of polypeptides containing the palindromic sequence AGAAAAGA may be rationalized by a delicate balance of the following three factors including (i) the extent of the zipper region, (ii) the number of hydrogen bonds, and (iii) the destabilizing effect of other bulky residues to the zipper region. Together with other biochemical results which indicate that the AGAAAAGA region is solvent exposed, the strong hydrophobic interaction of this palindromic region may be associated with the infectivity of PrP^{Sc}.

ASSOCIATED CONTENT

Supporting Information

$^{13}C-^{13}C$ correlation spectrum of the sample of *AA*3, where the C′ of A117 and C^{β} of A120 are ^{13}C-labeled; a detailed description of how we construct the structural model for the $PrP_{113-127}$ fibrils. This material is available free of charge via the Internet at http://pubs.acs.org.

AUTHOR INFORMATION

Corresponding Author

*Phone: 886-2-33662994. Fax: 886-2-23636359. E-mail: chanjcc@ntu.edu.tw.

Funding

This work was supported by grants from the National Science Council and the Ministry of Education.

ACKNOWLEDGMENTS

We thank the reviewers for their helpful comments.

ABBREVIATIONS

SSNMR, solid-state nuclear magnetic resonance; MD, molecular dynamics; PrP^{C}, cellular prion protein; PrP^{Sc}, scrapie prion; FMOC, 9-fluorenylmethoxycarbonyl; TFA, trifluoroacetic acid; DI, deionized; TBME, *tert*-butyl methyl ether; MALDI-TOF, matrix-assisted laser desorption/ionization−time-of-flight; TEM, transmission electron microscopy; FT-IR, Fourier transform infrared; MAS, magic-angle spinning;

fpRFDR-CT, constant-time finite-pulse radio frequency driven dipolar recoupling.

REFERENCES

(1) Dobson, C. M. (2003) Protein folding and misfolding. *Nature 426*, 884−890.

(2) Chiti, F., and Dobson, C. M. (2006) Protein misfolding, functional amyloid, and human disease. *Annu. Rev. Biochem. 75*, 333−366.

(3) Tycko, R. (2006) Molecular structure of amyloid fibrils: insights from solid-state NMR. *Q. Rev. Biophys. 39*, 1−55.

(4) Heise, H. (2008) Solid-state NMR spectroscopy of amyloid proteins. *ChemBioChem 9*, 179−189.

(5) Chan, J. C. C. (2011) Solid-State NMR Techniques for the Structural Determination of Amyloid Fibrils. *Top. Curr. Chem.*, DOI: 10.1007/1128_2011_1154.

(6) Nelson, R., Sawaya, M. R., Balbirnie, M., Madsen, A. O., Riekel, C., Grothe, R., and Eisenberg, D. (2005) Structure of the cross-beta spine of amyloid-like fibrils. *Nature 435*, 773−778.

(7) Sawaya, M. R., Sambashivan, S., Nelson, R., Ivanova, M. I., Sievers, S. A., Apostol, M. I., Thompson, M. J., Balbirnie, M., Wiltzius, J. J. W., McFarlane, H. T., Madsen, A. O., Riekel, C., and Eisenberg, D. (2007) Atomic structures of amyloid cross-beta spines reveal varied steric zippers. *Nature 447*, 453−457.

(8) Petkova, A. T., Ishii, Y., Balbach, J. J., Antzutkin, O. N., Leapman, R. D., Delaglio, F., and Tycko, R. (2002) A structural model for Alzheimer's beta-amyloid fibrils based on experimental constraints from solid state NMR. *Proc. Natl. Acad. Sci. U. S. A. 99*, 16742−16747.

(9) Petkova, A. T., Yau, W. M., and Tycko, R. (2006) Experimental constraints on quaternary structure in Alzheimer's beta-amyloid fibrils. *Biochemistry 45*, 498−512.

(10) Sachse, C., Fandrich, M., and Grigorieff, N. (2008) Paired beta-sheet structure of an A beta(1−40) amyloid fibril revealed by electron microscopy. *Proc. Natl. Acad. Sci. U. S. A. 105*, 7462−7466.

(11) Ma, B., and Nussinov, R. (2002) Molecular dynamics simulations of alanine rich beta-sheet oligomers: Insight into amyloid formation. *Protein Sci. 11*, 2335−2350.

(12) Kuwata, K., Matumoto, T., Cheng, H., Nagayama, K., James, T. L., and Roder, H. (2003) NMR-detected hydrogen exchange and molecular dynamics simulations provide structural insight into fibril formation of prion protein fragment 106−126. *Proc. Natl. Acad. Sci. U. S. A. 100*, 14790−14795.

(13) Steinmetz, M. O., Gattin, Z., Verel, R., Ciani, B., Stromer, T., Green, J. M., Tittmann, P., Schulze-Bdese, C., Gross, H., van Gunsteren, W. F., Meier, B. H., Serpell, L. C., Muller, S. A., and Kammerer, R. A. (2008) Atomic models of de novo designed cc beta-met amyloid-like fibrils. *J. Mol. Biol. 376*, 898−912.

(14) Lee, S. W., Mou, Y., Lin, S.-Y., Chou, F.-C., Tseng, W.-H., Chen, C.-h., Lu, C.-Y. D., Yu, S. S.-F., and Chan, J. C. C. (2008) Steric Zipper of the Amyloid Fbrils Formed by Residues 109−122 of the Syrian Hamster Prion Protein. *J. Mol. Biol. 378*, 1142−1154.

(15) Madine, J., Jack, E., Stockley, P. G., Radford, S. E., Serpell, L. C., and Middleton, D. A. (2008) Structural insights into the polymorphism of amyloid-like fibrils formed by region 20−29 of amylin revealed by solid-state NMR and X-ray fiber diffraction. *J. Am. Chem. Soc. 130*, 14990−15001.

(16) Nielsen, J.T., Bjerring, M., Jeppesen, M. D., Pedersen, R. O., Pedersen, J. M., Hein, K. L., Vosegaard, T., Skrydstrup, T., Otzen, D. E., and Nielsen, N. C. (2009) Unique Identification of Supramolecular Structures in Amyloid Fibrils by Solid-State NMR Spectroscopy. *Angew. Chem., Int. Ed. 48*, 2118−2121.

(17) Walsh, P., Simonetti, K., and Sharpel, S. (2009) Core Structure of Amyloid Fibrils Formed by Residues 106−126 of the Human Prion Protein. *Structure 17*, 417−426.

(18) Wiltzius, J. J. W., Landau, M., Nelson, R., Sawaya, M. R., Apostol, M. I., Goldschmidt, L., Soriaga, A. B., Cascio, D., Rajashankar, K., and Eisenberg, D. (2009) Molecular mechanisms for protein-encoded inheritance. *Nat. Struct. Mol. Biol. 16*, 973−978.

(19) Petkova, A. T., Leapman, R. D., Guo, Z. H., Yau, W. M., Mattson, M. P., and Tycko, R. (2005) Self-propagating, molecular-level polymorphism in Alzheimer's beta-amyloid fibrils. *Science 307*, 262−265.

(20) Paravastua, A. K., Leapman, R. D., Yau, W. M., and Tycko, R. (2008) Molecular structural basis for polymorphism in Alzheimer's beta-amyloid fibrils. *Proc. Natl. Acad. Sci. U. S. A. 105*, 18349−18354.

(21) Riek, R., Hornemann, S., Wider, G., Billeter, M., Glockshuber, R., and Wuthrich, K. (1996) NMR structure of the mouse prion protein domain PrP(121−231). *Nature 382*, 180−182.

(22) Riek, R., Hornemann, S., Wider, G., Glockshuber, R., and Wuthrich, K. (1997) NMR characterization of the full-length recombinant murine prion protein, mPrP(23−231). *FEBS Lett. 413*, 282−288.

(23) Kocisko, D.A., Lansbury, P. T., and Caughey, B. (1996) Partial unfolding and refolding of scrapie-associated prion protein: Evidence for a critical 16-kDa C-terminal domain. *Biochemistry 35*, 13434−13442.

(24) Khalili-Shirazi, A., Summers, L., Linehan, J., Mallinson, G., Anstee, D., Hawke, S., Jackson, G. S., and Collinge, J. (2005) PrP glycoforms are associated in a strain-specific ratio in native PrP^{Sc}. *J. Gen. Virol. 86*, 2635−2644.

(25) Ernst, M., Samoson, A., and Meier, B. H. (2003) Low-power XiX decoupling in MAS NMR experiments. *J. Magn. Reson. 163*, 332−339.

(26) Ishii, Y. (2001) C-13-C-13 dipolar recoupling under very fast magic angle spinning in solid-state nuclear magnetic resonance: Applications to distance measurements, spectral assignments, and high-throughput secondary-structure determination. *J. Chem. Phys. 114*, 8473−8483.

(27) Delaglio, F., Grzesiek, S., Vuister, G. W., Zhu, G., Pfeifer, J., and Bax, A. (1995) Nmrpipe - a Multidimensional Spectral Processing System Based on Unix Pipes. *J. Biomol. NMR 6*, 277−293.

(28) Goddard, T. D., and Kneller, C. G. Sparky, 3, University of California, San Francisco, http://www.cgl.ucsf.edu/home/sparky/.

(29) Ishii, Y., Balbach, J. J., and Tycko, R. (2001) Measurement of dipole-coupled lineshapes in a many-spin system by constant-time two-dimensional solid state NMR with high- speed magic-angle spinning. *Chem. Phys. 266*, 231−236.

(30) Bak, M., Rasmussen, J. T., and Nielsen, N. C. (2000) SIMPSON: A general simulation program for solid-state NMR spectroscopy. *J. Magn. Reson. 147*, 296−330.

(31) Veshtort, M., and Griffin, R. G. (2006) SPINEVOLUTION: A powerful tool for the simulation of solid and liquid state NMR experiments. *J. Magn. Reson. 178*, 248−282.

(32) Ponder, J. W. (2004) Tinker Software Tools for Molecular Design, Version 4.2, http:\\dasher.wustl.edu\tinker.

(33) Cornell, W. D., Cieplak, P., Bayly, C. I., Gould, I. R., Merz, K. M., Ferguson, D. M., Spellmeyer, D. C., Fox, T., Caldwell, J. W., and Kollman, P. A. (1995) A 2nd Generation Force-Field for the Simulation of Proteins, Nucleic-Acids, and Organic-Molecules. *J. Am. Chem. Soc. 117*, 5179−5197.

(34) Ooi, T., Oobatake, M., Nemethy, G., and Scheraga, H. A. (1987) Accessible Surface-Areas as a Measure of the Thermodynamic Parameters of Hydration of Peptides. *Proc. Natl. Acad. Sci. U. S. A. 84*, 3086−3090.

(35) Essmann, U., Perera, L., Berkowitz, M. L., Darden, T., Lee, H., and Pedersen, L. G. (1995) A Smooth Particle Mesh Ewald Method. *J. Chem. Phys. 103*, 8577−8593.

(36) Andersen, H. C. (1983) Rattle - a Velocity Version of the Shake Algorithm for Molecular-Dynamics Calculations. *J. Comput. Phys. 52*, 24−34.

(37) The PyMOL Molecular Graphics System, Version 1.3r1, Schrödinger, LLC., http://www.pymol.org.

(38) Koradi, R., Billeter, M., and Wuthrich, K. (1996) MOLMOL: A program for display and analysis of macromolecular structures. *J. Mol. Graph. 14*, 51−55.

(39) Hiramatsu, H., and Kitagawa, T. (2005) FT-IR approaches on amyloid fibril structure. *Biochim. Biophys. Acta 1753*, 100−107.

(40) Paul, C., and Axelsen, P. H. (2005) Beta sheet Structure in Amyloid Beta Fibrils and Vibrational Dipolar Coupling. *J. Am. Chem. Soc. 127*, 5754−5755.

(41) Antzutkin, O. N., Balbach, J. J., Leapman, R. D., Rizzo, N. W., Reed, J., and Tycko, R. (2000) Multiple quantum solid-state NMR indicates a parallel, not antiparallel, organization of beta-sheets in Alzheimer's beta- amyloid fibrils. *Proc. Natl. Acad. Sci. U. S. A. 97*, 13045−13050.

(42) Decatur, S. M. (2006) Elucidation of residue-level structure and dynamics of polypeptides via isotopp-edited infrared spectroscopy. *Acc. Chem. Res. 39*, 169−175.

(43) Petty, S. A., Adalsteinsson, T., and Decatur, S. M. (2005) Correlations among morphology, ss-sheet stability, and molecular structure in prion peptide aggregates. *Biochemistry 44*, 4720−4726.

(44) Silva, R. A. G. D., Barber-Armstrong, W., and Decatur, S. M. (2003) The organization and assembly of a beta-sheet formed by a prion peptide in solution: an isotope-edited FTIR study. *J. Am. Chem. Soc. 125*, 13674−13675.

(45) Karjalainen, E. L., Ravi, H. K., and Barth, A. (2011) Simulation of the Amide I Absorption of Stacked beta-Sheets. *J. Phys. Chem. B 115*, 749−757.

(46) Wishart, D. S., Bigam, C. G., Holm, A., Hodges, R. S., and Sykes, B. D. (1995) 1H, 13C and 15N random coil NMR chemical shifts of the common amino acids. I. Investigation of nearest-neighbor effects. *J. Biomol. NMR 5*, 67−81.

(47) Balbach, J. J., Petkova, A. T., Oyler, N. A., Antzutkin, O. N., Gordon, D. J., Meredith, S. C., and Tycko, R. (2002) Supramolecular structure in full-length Alzheimer's beta- amyloid fibrils: Evidence for a parallel beta-sheet organization from solid-state nuclear magnetic resonance. *Biophys. J. 83*, 1205−1216.

(48) Nguyen, H. D., and Hall, C. K. (2004) Molecular dynamics simulations of spontaneous fibril formation by random-coil peptides. *Proc. Natl. Acad. Sci. U. S. A. 101*, 16180−16185.

(49) Nguyen, H. D., and Hall, C. K. (2006) Spontaneous fibril formation by polyalanines; Discontinuous molecular dynamics simulations. *J. Am. Chem. Soc. 128*, 1890−1901.

(50) Gasset, M., Baldwin, M. A., Lloyd, D. H., Gabriel, J. M., Holtzman, D. M., Cohen, F. E., Fletterick, R. J., and Prusiner, S. B. (1992) Predicted alpha-helical regions of the prion protein when synthesized as peptides form amyloid. *Proc. Natl. Acad. Sci. U. S. A. 89*, 10940−10944.

(51) Helmus, J. J., Surewicz, K., Surewicz, W. K., and Jaroniec, C. P. (2010) Conformational Flexibility of Y145Stop Human Prion Protein Amyloid Fibrils Probed by Solid-State Nuclear Magnetic Resonance Spectroscopy. *J. Am. Chem. Soc. 132*, 2393−2403.

(52) Helmus, J. J., Surewicz, K., Nadaud, P. S., Surewicz, W. K., and Jaroniec, C. P. (2008) Molecular conformation and dynamics of the Y145Stop variant of human prion protein in amyloid fibrils. *Proc. Natl. Acad. Sci. U. S. A. 105*, 6284−6289.

(53) Tycko, R., Savtchenko, R., Ostapchenko, V. G., Makarava, N., and Baskakov, I. V. (2010) The alpha-Helical C-Terminal Domain of Full-Length Recombinant PrP Converts to an In-Register Parallel beta-Sheet Structure in PrP Fibrils: Evidence from Solid-State Nuclear Magnetic Resonance. *Biochemistry 49*, 9488−9497.

(54) Szeverenyi, N. M., Sullivan, M. J., and Maciel, G. E. (1982) ^{13}C Spin exchange by 2D FT ^{13}C CP/MAS. *J. Magn. Reson. 47*, 462−475.